Estuarine, Coastal and Shelf Science (2001) **53,** 801–812
doi:10.1006/ecss.2000.0730, available online at http://www.idealibrary.com on IDEAL®

Combined Use of Remote Sensing and Continuous Monitoring to Analyse the Variability of Suspended-Sediment Concentrations in San Francisco Bay, California

C. A. Ruhl[a], D. H. Schoellhamer[a], R. P. Stumpf[b] and C. L. Lindsay[c]

[a]*U.S. Geological Survey, 6000 J Street, Placer Hall, Sacramento, CA 95819, U.S.A.*
[b]*National Oceanic and Atmospheric Administration, 1305 East-West Highway, Silverspring, MD 20910, U.S.A.*
[c]*State Water Resources Control Board, State Division of Water Rights, 1001 I Street, P.O. Box 2000, Sacramento, CA 95812-2000, U.S.A.*

Received 6 December 1999, and accepted in revised form 14 September 2000

Analysis of suspended-sediment concentration data in San Francisco Bay is complicated by spatial and temporal variability. *In situ* optical backscatterance sensors provide continuous suspended-sediment concentration data, but inaccessibility, vandalism, and cost limit the number of potential monitoring stations. Satellite imagery reveals the spatial distribution of surficial-suspended sediment concentrations in the Bay; however, temporal resolution is poor. Analysis of the *in situ* sensor data in conjunction with the satellite reflectance data shows the effects of physical processes on both the spatial and temporal distribution of suspended sediment in San Francisco Bay. Plumes can be created by large freshwater flows. Zones of high suspended-sediment concentrations in shallow subembayments are associated with wind-wave resuspension and the spring-neap cycle. Filaments of clear and turbid water are caused by different transport processes in deep channels, as opposed to adjacent shallow water.

Keywords: suspended-sediment; estuary; satellite imagery; continuous monitoring; remote sensing; San Francisco Bay

Introduction

San Francisco Bay is comprised of several major subembayments: South San Francisco Bay (South Bay), Central San Francisco Bay (Central Bay), San Pablo Bay, and Suisun Bay (Figure 1). The Bay has semidiurnal tides that range from 1·7 metres (m) in Suisun Bay, to 2·0 m at the Golden Gate Bridge and in Central Bay, and 3·0 m in South Bay. The tides also have a pronounced 14-day spring-neap cycle: at the Golden Gate the maximum spring tidal range is 2·6 m and the minimum neap tidal range is 0·5 m. Typical tidal currents in the Bay range from 0·2 metres per second ($m\ s^{-1}$) in shallow water (depths <3 m) to more than 0·9 $m\ s^{-1}$ in deep-water channels (depths >3 m) (Cheng & Gartner, 1984). Winds typically are strongest during the summer when there is an afternoon onshore sea breeze. Most precipitation occurs from late autumn to early spring, with the greatest freshwater discharge into the Bay occurring during the spring, due to snowmelt runoff. About 90% of the discharge is drainage from the Central Valley watershed that passes through the Sacramento-San Joaquin Delta and enters the Bay at Mallard Island (Figure 1) (Smith, 1987).

Discharge from the Central Valley watershed contains 83–86% of the fluvial sediments that enter the Bay (Porterfield, 1980). During wet winters, turbid plumes of water arriving from the Central Valley watershed have extended into South Bay (Carlson & McCulloch, 1974). Turbidity maxima in Suisun Bay are dependent on the longitudinal salinity gradient and bottom topography (Schoellhamer & Burau, 1998). Suspended-sediment concentrations (SSC) also are affected by tidal currents, particularly during the more energetic spring tides, and by wind-wave resuspension in shallow water (Powell *et al.*, 1989; Schoellhamer, 1996).

Sediment is an important component of the San Francisco Bay estuarine system. The bottom sediments in South Bay and in the shallow waters of Central, San Pablo, and Suisun Bays are mostly composed of silts and clays. Silts and sands are present in the deeper parts of Central, San Pablo, and Suisun Bays and in Carquinez Straits (Conomos & Peterson, 1977). Particles in suspension are

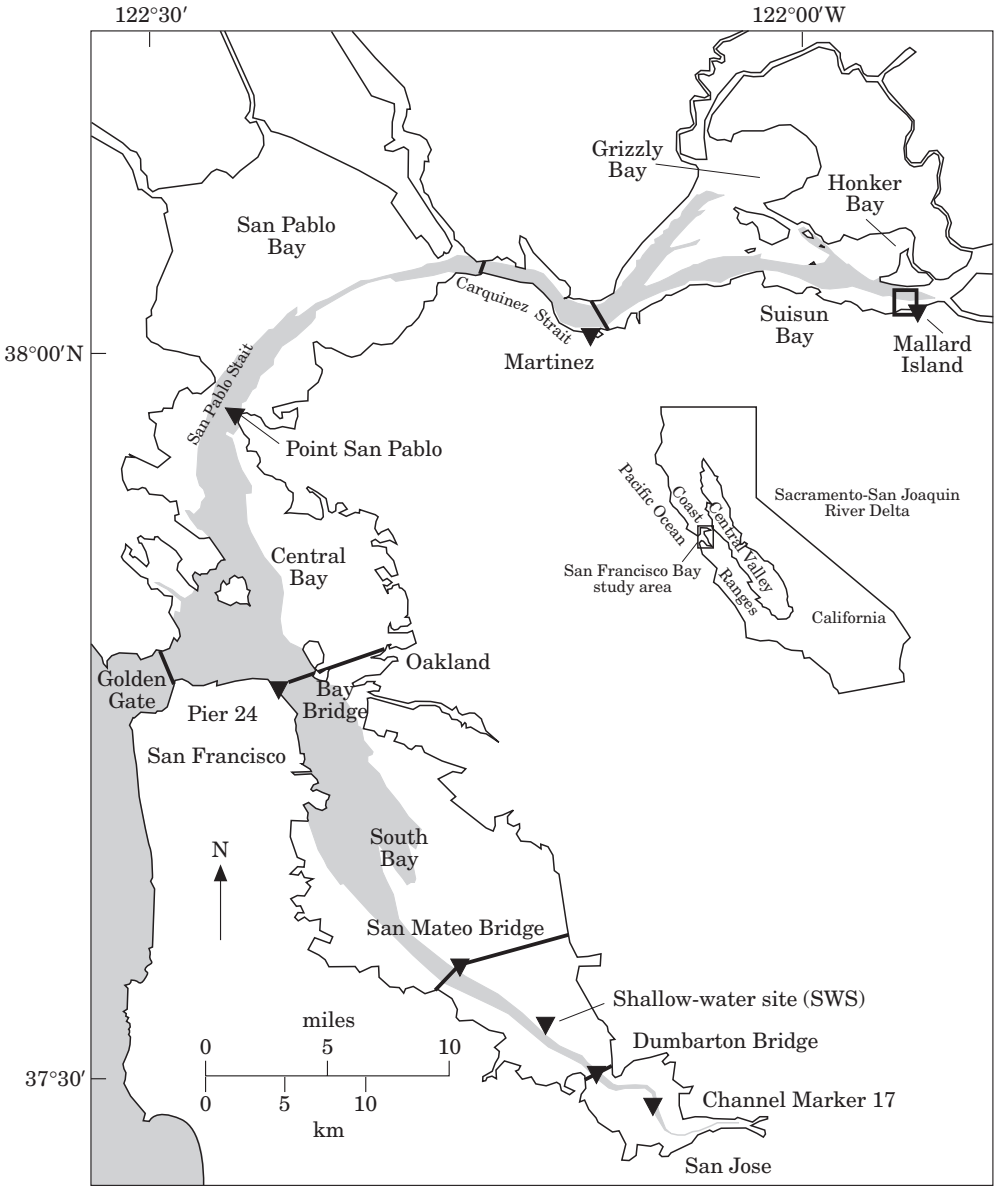

FIGURE 1. Study area, San Francisco Bay, California. ▼, Suspended-sediment concentration monitoring station; □, Suisun Bay meteorological station; ▩, Depth greater than 6 metres.

predominantly fine sediments that are flocculated (Krank & Milligan, 1992). Bottom sediments provide habitat for benthic organisms and are a source of nutrients that contribute to the maintenance of estuarine productivity (Hammond *et al.*, 1985). Potentially toxic substances, such as metals and pesticides, adsorb to sediment particles (Kuwabara *et al.*, 1989; Domagalski & Kuivila, 1993; Flegal *et al.*, 1996) and can be introduced into the food web through ingestion by benthic organisms (Luoma *et al.*, 1985; Brown & Luoma, 1995).

Spatial and temporal variations of SSC in San Francisco Bay are affected by turbulence, semidiurnal tides, the spring-neap cycle, seasonal winds, and freshwater flows. Each of these processes acts on a different time scale, ranging from seconds to years, and affects SSC differently, depending on the local bathymetric and physical environment (Cloern & Nichols, 1985).

Design of a sampling programme to understand how these physical processes affect SSC is complicated by spatial and temporal variability. A synthesis of high-resolution temporal SSC data combined with the areal coverage of satellite imagery provides the information needed to document the physical processes controlling SSC in the Bay.

Data collection

Two data sets were utilized in the preparation of this paper. Optical sensors collected continuous SSC data at eight locations in San Francisco Bay and satellites provided reflectance data with extensive spatial coverage of the Bay.

Continuous suspended-sediment concentration monitoring

The U.S. Geological Survey (USGS) continuously collected SSC, depth, salinity, and temperature data at upper and lower depths at seven long-term monitoring stations along the spine of the San Francisco Bay (Buchanan & Schoellhamer, 1998) and one short-term shallow water site (SWS) in South Bay (Buchanan, *et al.*, 1996) (Figure 1).

Optical backscatterance (OBS) sensors monitor concentrations of suspended sediment by transmitting a high-intensity infrared beam that is scattered or reflected by particles that are 0·5–30 centimetres in front of the optical window. Some of the light is reflected back through the window to a receiver and converted into a voltage output, proportional to the SSC at the sensor's depth (Downing, 1983). The data logger was programmed to power the optical sensors every 15 min, collect data every second for 1 min, and then average and store the output voltage for that 1-min period. USGS personnel visited the monitoring stations every 1–5 weeks to retrieve data, collect water samples for calibration, and remove biological fouling. Biological fouling, such as barnacle or bacterial growth, must be removed to avoid erroneous voltage outputs. The OBS sensor data set was processed to remove invalid data and anomalously high spikes.

Water samples, collected using a horizontally positioned Van Dorn sampler before and after sensor cleanings, were analysed for SSC. The Van Dorn sampler allows for a discrete sample to be taken at the same depth and time as an OBS sensor reading. A separate calibration for each OBS sensor was developed using ordinary least squares analysis of SSC measured in water samples versus the concurrent optical sensor measurements. The resulting calibration curves generally showed a good correlation between OBS sensor voltages and SSC; the coefficient of determination (R^2) ranged from 0·71 to 0·96 and the *t*-test for significance yielded *P*-values between the <0·001–0·002 levels (Buchanan & Schoellhamer, 1996; Buchanan *et al.*, 1996; Buchanan & Schoellhamer, 1998). The residual variance in the OBS calibrations is likely due to the inability of the Van Dorn sampler to collect the exact aliquot of water that the OBS sensor measures.

Satellite images

Advanced very high resolution radiometers (AVHRR) are mounted on the National Oceanic and Atmospheric Administration (NOAA)-12 and NOAA-14 polar orbiting weather satellites. Each satellite performs one overpass of the San Francisco Bay during daylight hours at approximately 0800 hours (h) (NOAA-12) and 1300h (NOAA-14) daily. All hourly values in this paper are referenced to Pacific Standard Time. The AVHRR sensor collects data in five broad bands of the electromagnetic spectrum; two visible light bands [red, 0·58–0·68 micrometres (μm) and near-infrared, 0·72–1·1 μm] and three thermal infrared bands (Stumpf, 1991).

Forty-three satellite images taken between 12 March 1994 and 9 February 1998 were spatially registered to a Mercator map projection with a pixel size of approximately 1 square kilometre (km^2). Clouds were identified and marked on each satellite image using a combination of thermal bands 4 and 5 and visible band 1. Radiance values for bands 1 and 2 were calibrated to correct for AVHRR sensor drift (Stumpf & Frayer, 1997) and processed to water reflectance with correction for atmospheric Rayleigh and aerosol effects and solar zenith angle (Stumpf & Pennock, 1989). Suspended particles increase water reflectance.

To relate AVHRR reflectance to SSC, each continuous monitoring station was identified on the satellite images using the station's latitude and longitude coordinates and selecting the reflectance in the pixel closest to the station that appeared to have no land influence. Land severely reduced the reflectance. The Mallard Island, Martinez, and Dumbarton Bridge stations are located in narrow reaches of the Bay and the Channel Marker 17 station is located near some tidal mud flats; these stations were excluded from consideration because of excessive land influence. The Point San Pablo, Pier 24, and San Mateo Bridge stations are located in open areas with little or no land interference, and were used to develop the AVHRR reflectance relation to SSC. Over the duration of the study these sites had 72%, 42%, and 31% valid OBS time-series data respectively.

AVHRR reflectance was related to SSC data from the upper *in situ* OBS sensors at the time nearest to the satellite overpasses. Only the data collected from the upper OBS sensors were used in this analysis because the high turbidity of the Bay attenuates light and

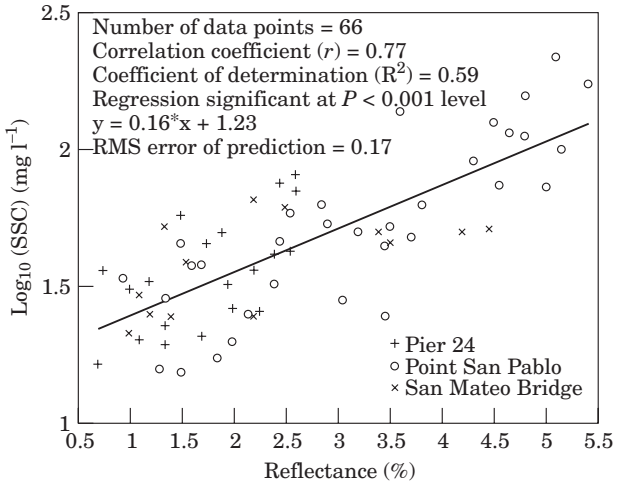

FIGURE 2. Relation between reflectance and suspended-sediment concentration in San Francisco Bay, California. RMS, root-mean square; mg l^{-1}, milligrams per litre; SSC, suspended-sediment concentration.

limits AVHRR sensor sensitivity to no more than the uppermost 1 m of the water column. This is an important limitation of this method because the depth of the upper OBS sensors used in this analysis ranged from 3 to 6 m below mean lower-low water. Although there is rapid light attenuation in San Francisco Bay, the patterns of variation discussed here probably extend below the uppermost 1 m of the water column. Analysis of 237 vertical profiles collected by Baylosis *et al.* (1997) during this study show that the SSC in the uppermost meter of the water column correlates well with the SSC measured 5 m below the surface with an R^2 of 0·84. The relation between AVHRR reflectance and SSC, plotted as percent reflectance versus log SSC (Stumpf & Pennock, 1989), resulted in an R^2 of 0·59 and the *t*-test for significance yielded *P*-values of $P<0{\cdot}001$ (Figure 2). All SSC values taken from the satellite images are reported as ranges rather than absolute values.

Although the relationship between AVHRR reflectance and SSC is not as good as that between OBS sensor voltage and SSC, there is a definite correlation. This relation was used to assign an SSC value to each pixel on the satellite image. Many factors complicate the establishment of a relation between AVHRR reflectance and SSC: spatial variability between 1-km^2 pixels and point measurements; vertical gradients, where surficial SSC measured by AVHRR reflectance may differ significantly from *in situ* sensor data collected lower in the water column; and interference with AVHRR reflectance from cloud cover, fog, and spring chlorophyll blooms (Stumpf & Tyler, 1988).

Results

Satellite imagery was used to map the spatial distribution of surficial SSC and to identify unique reflectance signatures associated with specific physical processes. Plumes can be created by high freshwater flows. Zones of high SSC in shallow subembayments are associated with wind-wave resuspension and the spring-neap cycle. Filaments of clear and turbid water are caused by the differing transport processes in deep channels as opposed to adjacent shallow water. Although these physical processes are well documented, satellite imagery provides added insight to the areal extent of these processes.

Plumes

Elevated sediment loads are frequently associated with the ‘ first flush ’, in which the easily erodible sediment from the Central Valley watershed is washed into the San Francisco Bay generating a moving slug of suspended sediment (Goodwin & Denton, 1991; Oltmann *et al.*, 1999). On 13 March 1995, a freshwater flood pulse arrived at the Mallard Island station and Delta outflow peaked at 11 500 cubic metres per second ($m^3 s^{-1}$) (California Department of Water Resources, 1986). Prior to the pulse, SSC values were low at the Martinez, Point San Pablo, and San Mateo Bridge stations. After the pulse, SSC increased at all stations, most dramatically at the Point San Pablo station (Figure 3). Biological fouling and equipment failure caused data loss at the San Mateo Bridge station after the initial increase in SSC; however, it is assumed that the SSC at the San Mateo Bridge and South Bay generally was on a downward trend at that time.

Comparison of data from the Martinez and Point San Pablo stations shows the progression of a turbid plume due to high freshwater flows (Figure 3). The pattern seen in the OBS sensor data is a classic pattern of plume progression; continuous temporal data track the sediment pulse from the Delta through Suisun and Central Bays (Figure 3). Concentrations at the Martinez station were driven strongly by river discharge, with a peak in SSC nearly coincident with the flood pulse. SSC at the Point San Pablo station increased 1–2 days later and showed strong spiking with the tide and peaks higher than upstream SSC at the Martinez station. The response seen at the Point San Pablo station probably is the result of resuspension of the newly deposited sediments in neighbouring shallows and subsequent advection past the sensor.

Two satellite images of San Francisco Bay taken during ebb tide, 6 March at 0700h and 25 March at

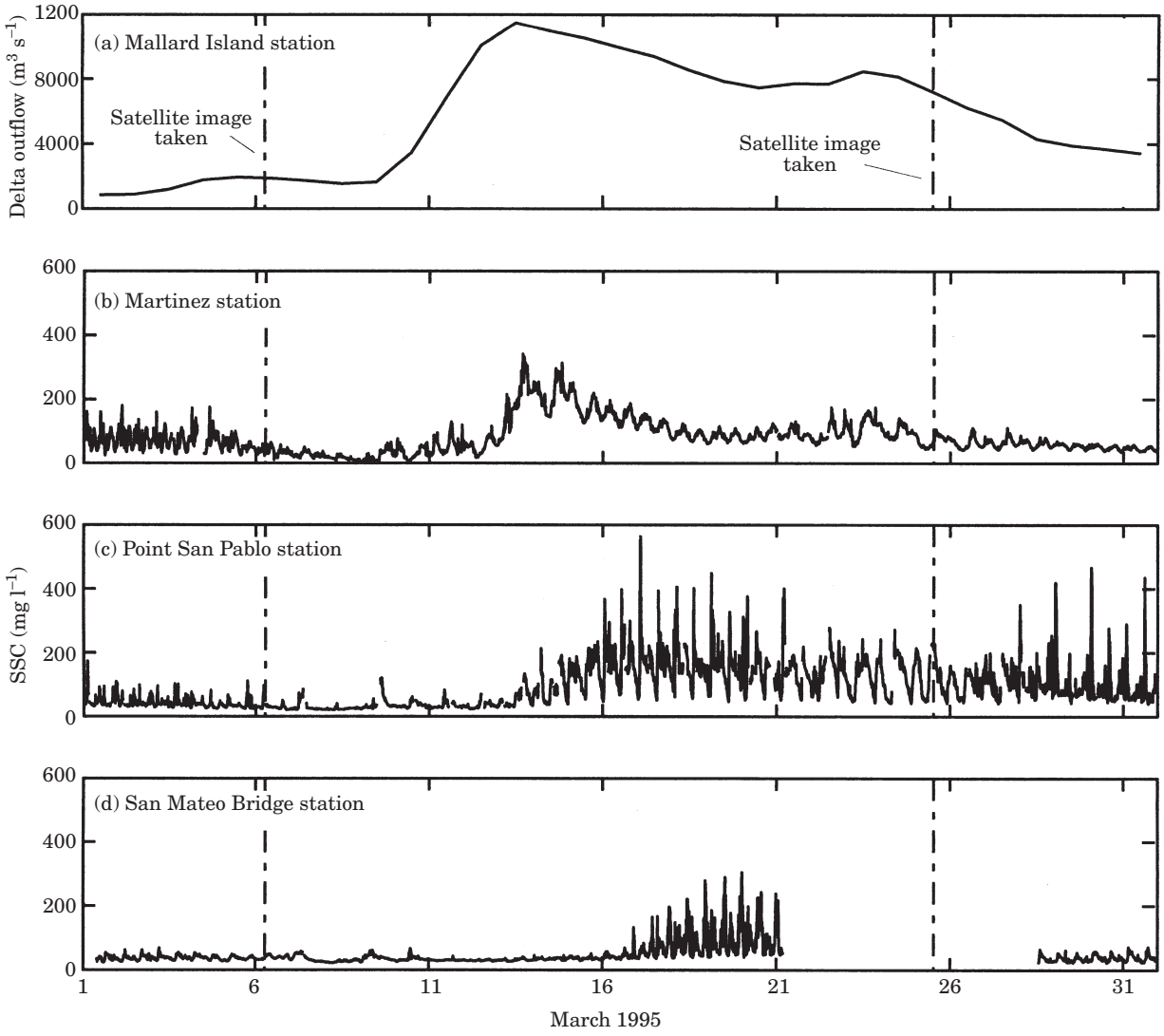

FIGURE 3. Comparison of Delta outflow at Mallard Island station (a), and suspended-sediment concentration at the Martinez (b), Point San Pablo (c) and, San Mateo Bridge (d) stations, San Francisco Bay, California. $m^3 s^{-1}$, cubic metres per second; $mg l^{-1}$, milligrams per litre; SSC, suspended-sediment concentration.

1300h (Figure 4), show the spatial distribution of SSC in the upper 1 m of the water column before and after the freshwater and sediment pulse. The 6 March satellite image shows generally low SSC throughout the Bay with slightly higher SSC in the shallow areas of San Pablo Bay, Grizzly Bay, and the southern part of South Bay. Due to extensive cloud cover, another satellite image was not available until 25 March, which was 12 days after the pulse. The 25 March satellite image shows a plume of elevated SSC of 100–150 milligrams per litre ($mg l^{-1}$) travelling through the channels in Suisun and Central Bays and ultimately through the Golden Gate into the Pacific Ocean. Slightly higher concentrations are shown in South Bay on 25 March, which peaked at approximately 50–75 $mg l^{-1}$ at several locations.

Some suspended sediment moved into South Bay mid-March (Figure 3(d)], however, the image shows that the major conduit for the flow was through the Golden Gate [Figure 4(b)]. High freshwater discharge combined with ebb tides of approximately 1·5 $m s^{-1}$ at the Golden Gate produced a significant plume 10–15 km offshore. A much larger area was affected, as seen by an extensive region of 20–30 $mg l^{-1}$ SSC [turquoise area in Figure 4(b)] along the coast. Although the predicted ebb tide of approximately 1·8 $m s^{-1}$ at the Golden Gate on 6 March was greater than the ebb tide on 25 March, there was no evidence of a suspended-sediment plume being carried through to the Pacific Ocean due to limited sediment availability prior to the freshwater pulse. Bottom sediments deposited during the winter tend to consolidate until

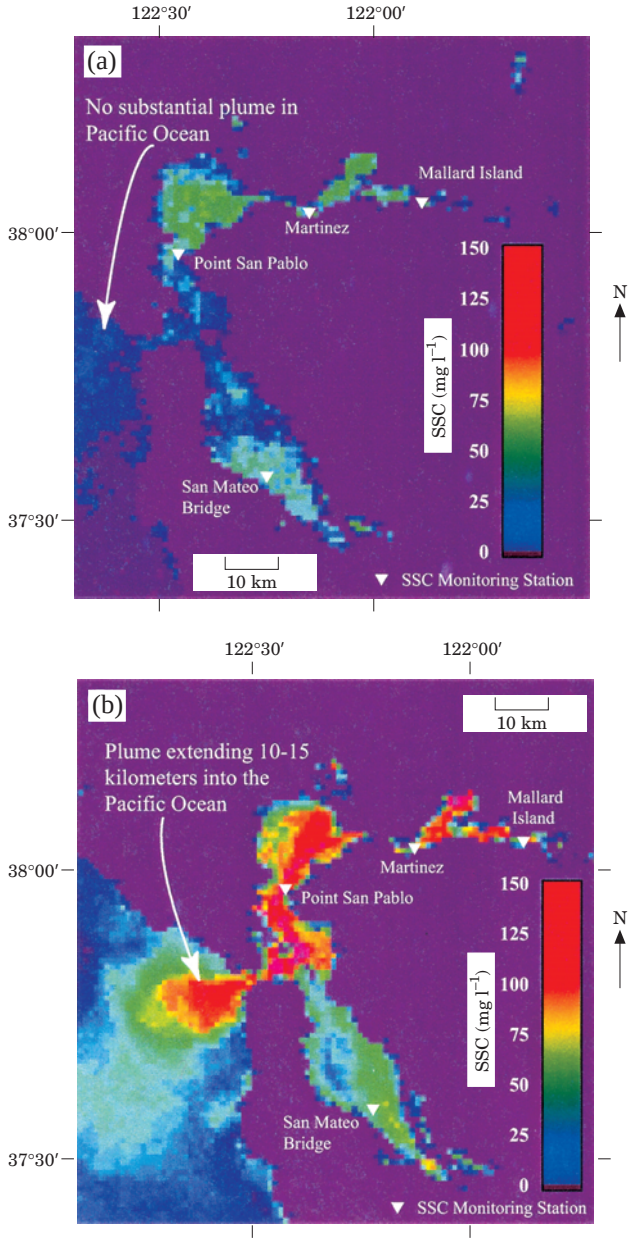

FIGURE 4. AVHRR images showing pre-flood conditions on 6 March 1995, at 0700h (a) and post-flood conditions on 25 March 1995, at 1300h (b), in San Francisco Bay, California. Both images were taken during ebb tide. SSC, suspended-sediment concentration; mg l^{-1}, milligrams per litre.

spring and summer, when wind-waves generate sufficient bottom shear stress to resuspend the sediment (Krone, 1979). However, new sediments from a freshwater pulse, such as those seen in the 25 March satellite image, are more susceptible to resuspension by both wind-waves and tidal currents because consolidation is less.

Turbid subembayments

Shallow-water areas and deep channels display significantly different responses to physical forcings, such as the tidal cycle, wind-waves, and the spring-neap cycle (Ruhl & Schoellhamer, 1999). Resuspension of bed sediments tends to occur at low tide during windy periods, particularly during the higher sustained winds of early spring, when less consolidated bed sediment is more readily available for wind-wave resuspension. The effective bed-shear stress diminishes quickly with water depth; therefore, shallow waters experience significantly greater bed-shear stress than channels due to wind-waves, and more bed sediments are resuspended (Sanford, 1994; Schoellhamer, 1995; Jing & Ridd, 1996).

The spring-neap cycle is a well-documented physical process that affects SSC throughout San Francisco Bay (Schoellhamer, 1994, 1996). Water-level data show dominant spring tides during 9–14 July, neap tides during 17–21 July, and spring tides during late July [Figure 5(c)]. Optical sensor data collected at the Point San Pablo station in 1995 showed a correlation between the spring-neap cycle and SSC [Figure 5(a)]. SSC tends to increase during spring tides and decrease during the less energetic neap tides.

The spring-neap cycle that is apparent in the OBS sensor data also is apparent in the satellite images. Areas of turbid water with SSC of 100–150 mg l^{-1} appeared in northern San Pablo Bay on both spring-tide satellite images, taken on 15 and 30 July [Figure 6(a) and (c)], with notably higher SSC in San Pablo Bay on 15 July after the large spring tide. Significantly lower SSC was observed in San Pablo Bay during the neap tides, as seen in the 23 July satellite image [Figure 6(b)]. The highest levels of SSC were in the northern and northwestern parts of San Pablo Bay, where depths generally are less than 2 m. The channel along the southern boundary of San Pablo Bay, near the Point San Pablo station, reaches depths of more than 12 m and had substantially lower SSC.

Continuous westerly winds generally prevail during the spring and summer in San Francisco Bay. Wind speed averaged 7·3 m s^{-1} in Suisun Bay (Suisun Bay Meteorological Station data) 10 July–5 August, 1995. The highest winds occurred during the neap tides, but only a limited response is shown in both the OBS sensor data and satellite images (Figures 5 and 6) due to generally deeper water. The 15 and 30 July satellite images were taken following spring-tide periods that succeeded a windy period [Figure 5(b) and (c)]. Sediments, resuspended during the windy period that preceded the satellite flyover, could have remained in suspension due to the more energetic spring tides.

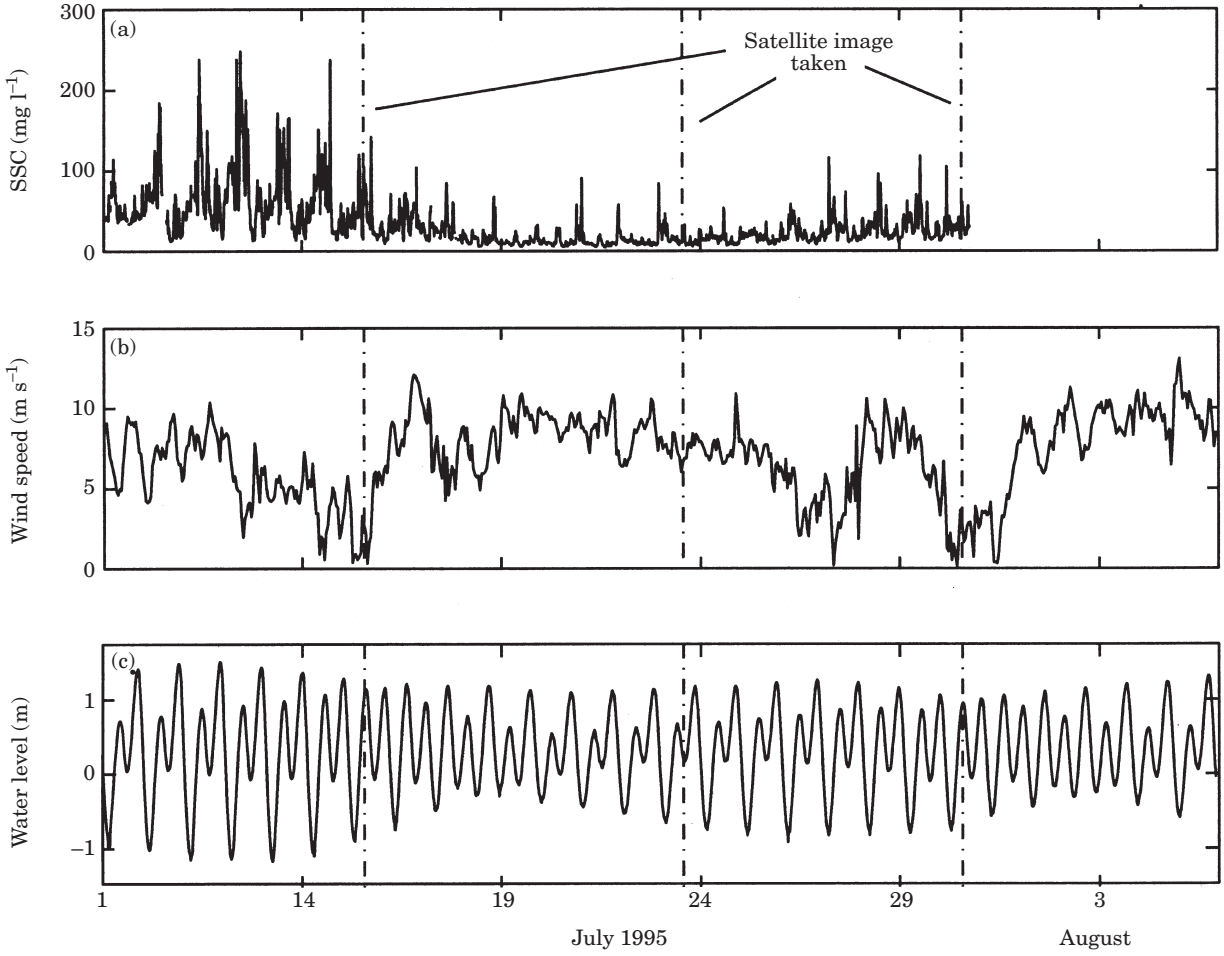

FIGURE 5. SSC, suspended-sediment concentration at the Point San Pablo station (a); westerly wind speed at the Suisun Bay Meteorological Station (b); and water level, measured from a zero datum of sea level as defined by the National Geodetic Vertical Datum of 1929, at the Point San Pablo station (c). mg l^{-1}, milligrams per litre; m s^{-1}, metres per second; m, metres.

Filaments

Transport mechanisms in channels are different to those in shallow areas. Shallow areas tend to act as temporary sediment-storage zones (Ruhl & Schoellhamer, 1999). Unconsolidated bottom sediments in shallow areas are winnowed slowly from the bed and carried to neighbouring channels (Krone, 1979; Nichols & Thompson, 1985). Channels in San Francisco Bay are the primary transport arteries connecting subembayments to the Golden Gate, and the higher velocities in the channels tend to carry suspended sediment greater distances.

Images taken at 0800h and 1300h on 30 July 1995 highlight the effect of the differing transport characteristics of channels and shallows (Figure 7). The satellite image taken at 0800h [Figure 7(a)] shows that suspended sediments from the shallows of South Bay were advected into the north-south trending channel near its western shore. The high velocities generated during ebb tide created a filament of relatively turbid water with SSC of 25–50 mg l^{-1} that extended northward toward the Golden Gate. A similar phenomenon occurred during flood tide in Central Bay and was captured by the satellite image taken at 1300h [Figure 7(b)]. A filament of relatively clear Pacific Ocean water appeared in the deep channel in San Pablo Bay and penetrated up to Carquinez Strait.

In addition to filaments, these two images show the significant variability in suspended-sediment distribution over a 5-h period. At 0800h, an ebb tide transported sediment through the Golden Gate, creating a small plume of slightly elevated SSC offshore; this plume was not present during the flood tide at 1300h. Another significant difference between the two images is in the San Pablo Bay region; the highest

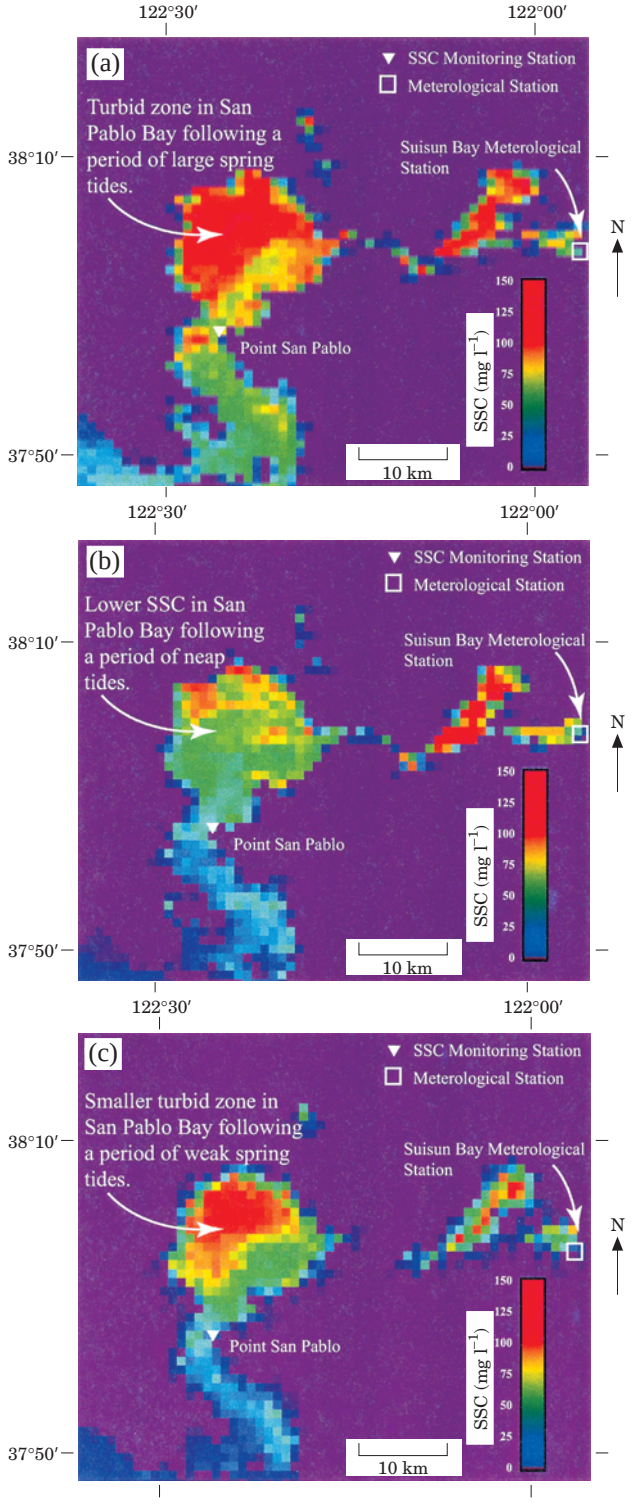

FIGURE 6. AVHRR images showing suspended-sediment concentrations at the end of large spring tidal period on 15 July 1995, at 1300h (a); at the end of neap tidal period on 23 July 1995, at 1300h (b); and at the end of weak spring tidal period on 30 July 1995, at 1300h (c), in San Francisco Bay, California. SSC, suspended-sediment concentration; mg l^{-1}, milligrams per litre.

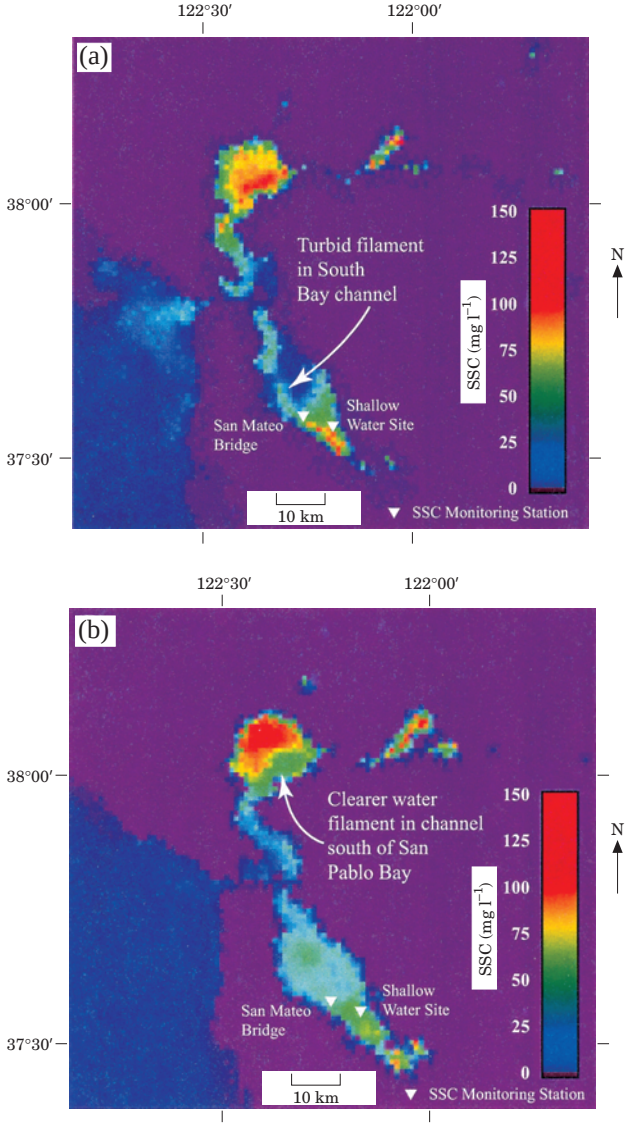

FIGURE 7. AVHRR images showing relatively turbid and relatively clear filaments in San Francisco Bay, California. A turbid filament, as compared to the less turbid shallows, appears in the South Bay channel on 30 July 1995, at 0800h (a); and a relatively clear water filament, as compared to the neighbouring highly turbid shallows, appears in the channel south of San Pablo Bay on 30 July 1995, at 1300h (b). SSC, suspended-sediment concentration; mg l^{-1}, milligrams per litre.

SSC was seen during ebb tide at 0800h in the deep channel. During the flood tide at 1300 h, the highest SSC was in the northern shallows. This shift of the zone of high SSC shows the interaction between channels and shallows over a tidal cycle.

Optical sensor data collected from the San Mateo Bridge station and SWS, a shallow-water station located in South Bay during the spring of 1994 (Figure 1), show similar patterns (Schoellhamer,

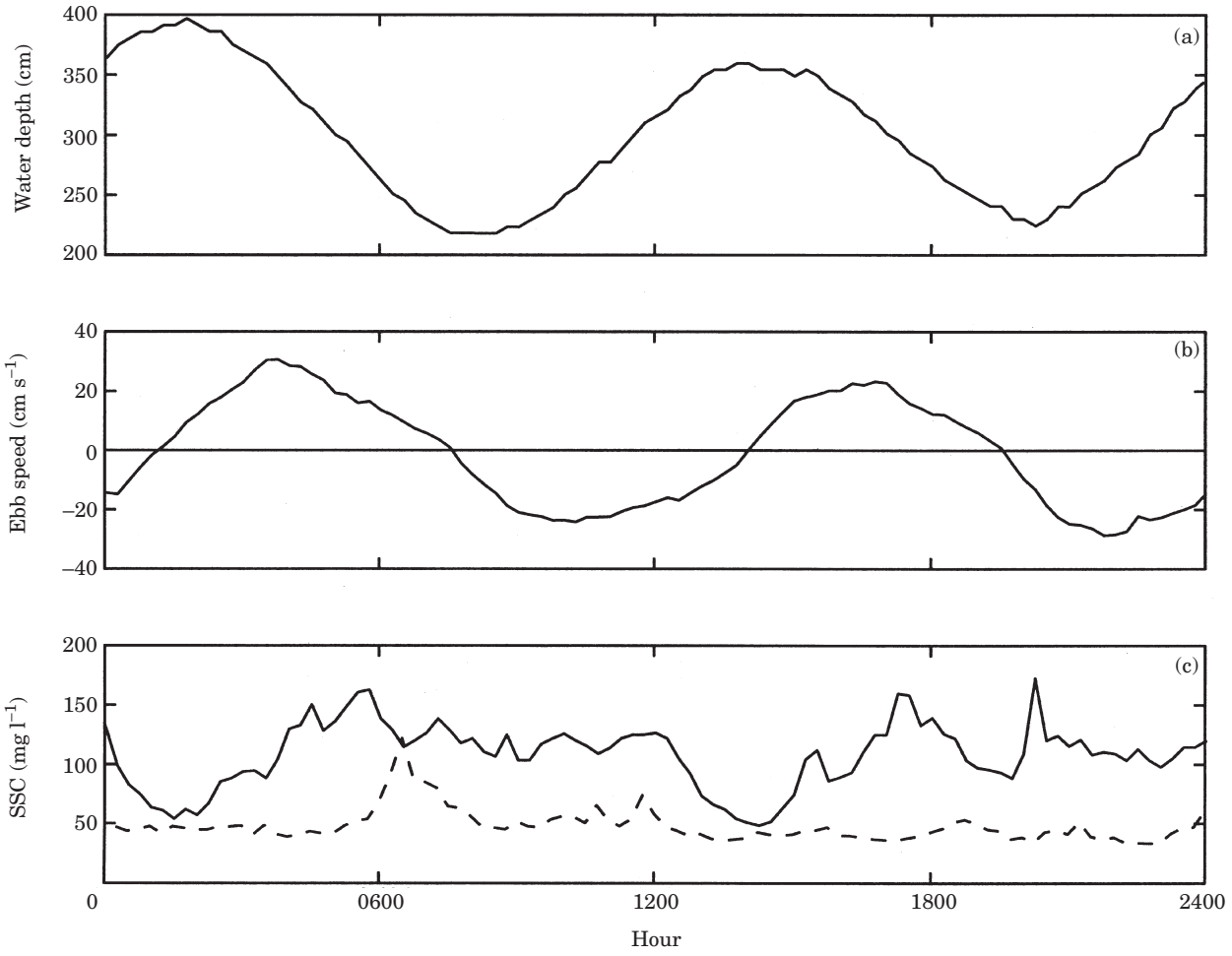

FIGURE 8. Comparison of data at two locations on 15 March 1994: the shallow-water station and the San Mateo Bridge station in South San Francisco Bay, California (Schoellhamer, 1996). Water depth at the shallow-water station (a); ebb speed at the shallow-water station (b); and suspended-sediment concentrations at the shallow-water station and the San Mateo Bridge station (c). cm, centimetres; cm s^{-1}, centimetres per second; mg l^{-1}, milligrams per litre; ——, SWS, shallow-water station; – – –, SMB, San Mateo Bridge.

1996). With the onset of a large ebb tide, SSC at SWS peaked at approximately 150 mg l^{-1} just after maximum ebb tide (Figure 8). A plateau of 100–150 mg l^{-1} SSC was maintained at SWS until just after the maximum flood tide with the arrival of clear water from the channel. SSC was reduced significantly for a short period before rising again with the onset of another ebb tide. The optical sensor data from the San Mateo Bridge station in the channel was dramatically different. Low SSC values were present at the San Mateo Bridge station until the end of an ebb tide, when the tidal excursion was large enough to transport resuspended sediment from the shallows into the channel and northward to the San Mateo Bridge. The peak of approximately 120 mg l^{-1} SSC at the San Mateo Bridge station was reversed quickly with the onset of flood tides. The second ebb tide on 15 March did not result in a peak in SSC at the San Mateo Bridge station, even though high SSC was seen at SWS. The ebb speed was lower during the second tidal cycle, suggesting that the tidal excursion was too small to transport the sediment to the San Mateo Bridge before the onset of flood tides.

Discussion

The combination of *in situ* OBS sensor data and satellite imagery expands our understanding of the physical processes controlling SSC in San Francisco Bay. Unique reflectance signatures seen in satellite images were identified and linked to specific processes observed with optical sensors. Plumes seen in satellite images demonstrate the dominant transport mechanisms during high freshwater flows and ebb tides.

Zones of elevated SSC in shallow subembayments vary with the spring-neap cycle. Filaments reveal the difference in transport characteristics between channels and shallows.

The variability in SSC observed at the surface is likely to be present throughout the water column. SSC is greater near the bottom due to resuspension and particle settling, but the temporal and horizontal variability of SSC is likely to be similar at the surface and near the bottom. Plumes of turbid freshwater typically are well-mixed because salinity stratification is absent. An exception can occur where turbid freshwater is at the surface above clearer saltwater, but this is rare in this partially mixed estuary and has short duration because of particle settling. Zones of elevated SSC in shallow water are due to wind-wave resuspension of bottom sediment, and these shallow areas tend to be well mixed. Filaments are created by tidal advection of turbid or clear water that takes place throughout the water column.

While inaccessibility, vandalism, biological fouling, and cost are limitations of continuous-monitoring stations, satellite imagery has limitations as well. Cloud cover, fog, or a chlorophyll bloom can render a satellite image useless or call into question the validity of some of the data. Fog is particularly difficult to identify in satellite images. The inability to schedule satellite flyovers, daylight requirements for reflectance data, and frequency of images complicates the identification of phenomena that occur only at a specific time during the tidal cycle or occur at shorter time scales.

In addition to the limitations of each individual data-collection method, certain compatibility issues must be considered when combining these two methods. SSC is highly heterogeneous, therefore, a point value from a specific monitoring station may not represent the average SSC in an entire 1-km^2 pixel. The use of satellite imagery to estimate SSC at specific locations gives only approximate values, due to the large residual variance between reflectance and field-concentration data. Using a higher resolution image, such as 30-m resolution LANDSAT Thematic Mapper images, would greatly improve the compatibility of these two data-collection methods.

Vertical SSC gradients also may be a problem when comparing these satellite and OBS sensor data. The reflectance signal collected by the AVHRR sensor originates 1 m or less from the water surface; however, surface SSC often is quite different from mid-depth or bottom SSC. This variability in SSC through the water column is an important consideration when developing the AVHRR reflectance relation to SSC because the OBS sensors used in this study were placed more than 1 m below the water surface. Optimally, *in situ* optical sensors should be located in the top 1 m of the water column to establish the relation between AVHRR reflectance and SSC.

Finally, land interference in the AVHRR reflectance data must be considered. The reflectance of pixels immediately adjacent to land are contaminated by atmospheric adjacency and AVHRR sensor response; therefore, data from continuous monitoring stations near the coastline were difficult to relate to the AVHRR reflectance data. To minimize the effects of land interference on the relation between AVHRR reflectance and SSC, *in situ* optical sensors should be operating in open water areas far from the shoreline or tidal mudflats.

Conclusions

The combination of temporal suspended-sediment concentration (SSC) data and satellite imagery is valuable for analysing suspended-sediment transport in San Francisco Bay. Optical backscatterance (OBS) sensors provide SSC data with a high temporal resolution at point locations, whereas satellite imagery provides spatial coverage. This combination provides an effective means to analyse the physical processes governing suspended sediment transport, such as high freshwater flows, the spring-neap cycle, and differing transport processes in deep channels as opposed to adjacent shallow water. During ebb tide, suspended sediment can be transported by large freshwater pulses through the estuary, forming a plume in the Pacific Ocean. Turbid zones in subembayments appear and disappear with the spring-neap cycle. Filaments of turbid or clear water extend along the deep channels of the Bay, which are the primary pathways for longitudinal transport.

Acknowledgements

The authors thank Paul Buchanan, Robert Sheipline, Brad Sullivan, and Richard Adorador for operating the continuous monitoring stations. They gratefully acknowledge the support of the U.S. Army Corps of Engineers San Francisco District (as part of the Regional Monitoring Program for Trace Substances), the San Francisco Regional Water Quality Control Board, the USGS San Francisco Bay Place-Based Program, and the USGS Federal/State Cooperative Program. They also extend thanks to Robert Meyer, Gail Thelin, and Carol Sanchez of the USGS, Ray Krone from U.C. Davis, and the anonymous

reviewers for their many helpful comments during earlier versions of this article.

(The use of firm, trade and brand names in this report is for identification purposes only and does not constitute endorsement by the U.S. Geological Survey.)

References

Baylosis, J. I., Edmunds, J. L., Cole, B. E. & Cloern, J. E. 1997 Studies of the San Francisco Bay, California estuarine ecosystem. Pilot regional monitoring results, 1996: *U.S. Geological Survey Open-File Report 97-598*, 203 pp.

Brown, C. L. & Luoma, S. N. 1995 Use of the euryhaline bivalve *Potamocorbula amurensis* as a biosentinal species to assess trace metal contamination in San Francisco Bay. *Marine Ecology Progress Series*, **124,** pp. 129–142.

Buchanan, P. A. & Schoellhamer, D. H. 1996 Summary of suspended-solids concentration data, San Francisco Bay, California, water year 1995: *U.S. Geological Survey Open-File Report 96-591*, 40 pp.

Buchanan, P. A. & Schoellhamer, D. H. 1998 Summary of suspended-solids concentration data, San Francisco Bay, California, water year 1996: *U.S. Geological Survey Open-File Report 98-175*, 59 pp.

Buchanan, P. A., Schoellhamer, D. H. & Sheipline, R. C. 1996 Summary of suspended-solids concentration data, San Francisco Bay, California, water year 1994: *U.S. Geological Survey Open-File Report 95-776*, 48 pp.

California Department of Water Resources 1986 DAYFLOW program documentation and DAYFLOW data summary user's guide, http://www.iep.ca.gov/dayflow/data/.

Carlson, P. R. & McCulloch, D. S. 1974 Aerial observations of suspended-sediment plumes in San Francisco Bay and adjacent Pacific Ocean: *U.S. Geological Survey Water-Resources Research*, **2,** no. 5, pp. 519–526.

Cheng, R. T. & Gartner, J. W. 1984 Tides, tidal and residual currents in San Francisco Bay—Results of measurements, 1979–1980: *U.S. Geological Survey Water-Resources Investigations Report*, 84-4339, 72 pp.

Cloern, J. E. & Nichols, F. H. 1985 Time scales and mechanisms of estuarine variability, a synthesis from studies of San Francisco Bay. In *Temporal Dynamics of an Estuary-San Francisco Bay* (Cloern, J. E. & Nichols, F. H., eds). Dr. W. Junk Publishers, Boston, MA, U.S.A., pp. 229–237.

Conomos, T. J. & Peterson, D. H. 1977 *Suspended-particle transport and circulation in San Francisco Bay, an overview—Estuarine processes*. Academic Press, New York, **2,** pp. 82–97.

Domagalski, J. L. & Kuivila, K. M. 1993 Distributions of pesticides and organic contaminants between water and suspended sediment, San Francisco Bay, California. *Estuaries* **16,** 3A, 416–426.

Downing, P. P. 1983 An optical instrument for monitoring suspended particulates in ocean and laboratory. In OCEANS 1983, San Francisco, California, August 29–September 1, 1983. *Proceedings*, pp. 199–202.

Flegal, A. R., Rivera-Duarte, I., Ritson, P. I., Scelfo, G. M., Smith, G. J., Gordon, M. R. & Sanudo-Wilhelmy, S. A. 1996 Metal contamination in San Francisco Bay waters-historic perturbations, contemporary concentrations, and future considerations. In *San Francisco Bay—The ecosystem* (Hollibaugh, J. T., ed.). Pacific Division of the American Association for the Advancement of Science, San Francisco, pp. 173–188.

Goodwin, P. & Denton, R. A. 1991 Seasonal influences of the sediment transport characteristics of the Sacramento River, California: Institute of Civil Engineers. *Proceedings*, pt. 2, **91,** pp. 165–172.

Hammond, D. E., Fuller, C., Harmon, D., Hartman, B., Korosec, M., Miller, L. G., Rea, R., Warren, S., Berelson, W. & Hager, S. W. 1985 Benthic fluxes in San Francisco Bay. *Hydrobiologia* **129,** 69–90.

Jing, L. & Ridd, P. V. 1996 Wave-current bottom shear stresses and sediment resuspension in Cleveland Bay, Australia. *Coastal Engineering* **29,** 169–186.

Krank, K. & Milligan, T. G. 1992 Characteristics of suspended particles at an 11-hour anchor station in San Francisco Bay, California. *Journal of Geophysical Research* **97,** C7, 11373–11382.

Krone, R. B. 1979 Sedimentation in the San Francisco Bay system. In *San Francisco Bay–The urbanized estuary* (Conomos, T. J., ed.). Pacific Division of the American Association for the Advancement of Science, San Francisco, pp. 347–385.

Kuwabara, J. S., Chang, C. C. Y., Cloern, J. E., Fries, T. L., Davis, J. A. & Luoma, S. N. 1989 Trace metal associations in the water column of South San Francisco Bay, California. *Estuarine, Coastal and Shelf Science* **28,** 307–325.

Luoma, S. N., Cain, D. & Johansson, C. 1985 Temporal fluctuations of silver, copper, and zinc in the bivalve *Macoma balthica* at five stations in South San Francisco Bay. *Hydrobiologia* **129,** 109–120.

Nichols, R. H. & Thompson, J. K. 1985 Time scales of change in the San Francisco Bay benthos. *Hydrobiologia* **192,** 121–138.

Oltmann, R. N., Schoellhamer, D. H. & Dinehart, R. L. 1999 Sediment inflow to the Sacramento-San Joaquin Delta and the San Francisco Bay. *Interagency Ecological Program Newsletter* **12,** 30–33.

Porterfield, G. 1980 Sediment transport of streams tributary to San Francisco, San Pablo, and Suisun Bays, California, 1909–1966. *U.S. Geological Survey Water-Resources Investigations Report 80-64*, 91 pp.

Powell, T. M., Cloern, J. E. & Huzzey, L. M. 1989 Spatial and temporal variability in South San Francisco Bay (U.S.A.). Horizontal distributions of salinity, suspended sediments, and phytoplankton biomass and productivity. *Estuarine, Coastal and Shelf Science* **28,** 583–597.

Ruhl, C. A. & Schoellhamer, D. H. 1999 Time series of suspended-solids concentration in Honker Bay during water year 1997. *1997 Annual Report of the Regional Monitoring Program for Trace Elements*, pp. 82–92. (Url: http://www.sfei.org/rmp/1997/c0304.htm)

Sanford, L. P. 1994 Wave-forced resuspension of upper Chesapeake Bay muds. *Estuaries* **17,** 148–165.

Schoellhamer, D. H. 1994 Suspended-solids concentrations in central San Francisco Bay during 1993 winter runoff. *Eos Transactions of the American Geophysical Union* **75,** 122.

Schoellhamer, D. H. 1995 Sediment resuspension mechanisms in Old Tampa Bay, Florida. *Estuarine, Coastal and Shelf Science* **40,** 603–620.

Schoellhamer, D. H. 1996 Factors affecting suspended-solids concentrations in South San Francisco Bay, California. *Journal of Geophysical Research* **101,** C5, 12087–12095.

Schoellhamer, D. H. & Burau, J. R. 1998 Summary of findings about circulation and the estuarine turbidity maximum in Suisun Bay, California. *U.S. Geological Survey Fact Sheet FS-047-98*, 6 pp. (http://sfbay.wr.usgs.gov/access/suisunbay/dschoell/).

Smith, L. H. 1987 A review of circulation and mixing studies of San Francisco Bay, California. *U.S. Geological Survey Circular 1015*, 38 pp.

Stumpf, R. P. 1991 Observation of suspended sediments in Mobile Bay, Alabama, from satellite. *Coastal Sediments 1991 Specialty Conference, Water Resources Division of American Society of Civil Engineers*, Seattle, Washington, June 25–27 1991. *Proceedings*, pp. 789–802.

Stumpf, R. P. & Frayer, M. L. 1997 Application of AVHRR for examination of water clarity in time series in Florida Bay. In *Monitoring algal blooms: new techniques for detecting large-scale environmental change* (Kahru, M. & Brown, C. W., eds). Landes Bioscience, chapter 1, pp. 1–23.

Stumpf, R. P. & Pennock, J. R. 1989 Calibration of a general optical equation for remote sensing of suspended sediments in a moderately turbid estuary. *Journal of Geophysical Research* **94,** C10, 14363–14371.

Stumpf, R. P. & Tyler, M. A. 1988 Satellite detection of bloom and pigment distributions in estuaries. *Remote Sensing of the Environment* **24,** 385–404.